Nonlinear dynamics of the viscoelastic Kolmogorov flow

A. BISTAGNINO[1], G. BOFFETTA[1], A. CELANI[2], A. MAZZINO[3], A. PULIAFITO[2,3] AND M. VERGASSOLA[4]

[1]Dipartimento di Fisica Generale and INFN, Università di Torino,
via P. Giuria 1, 10125 Torino, Italy

[2]CNRS, INLN, 1361 Route des Lucioles, 06560 Valbonne, France

[3]Dipartimento di Fisica, Università di Genova, and CNISM, INFN, Sezione di Genova,
via Dodecaneso 33, 16146 Genova, Italy

[4]CNRS URA 2171, Inst. Pasteur, 25 rue du Dr Roux, 75724 Paris Cedex 15, France

The weakly nonlinear dynamics of large-scale perturbations in a viscoelastic flow is investigated both analytically, via asymptotic methods, and numerically. For sufficiently small elasticities, dynamics is ruled by a Cahn–Hilliard equation with a quartic potential. Physically, this amounts to saying that, for small elasticities, polymers do not alter the purely hydrodynamical mechanisms responsible for the nonlinear dynamics in the Newtonian case (i.e. without polymers). The approach to the steady state is quantitatively similar to the Newtonian case as well, the dynamics being ruled by the same kink–antikink interactions as in the Newtonian limit. The above scenario does not extend to large elasticities. We found a critical value above which polymers drastically affect the dynamics of large-scale perturbations. In this latter case, a new dynamics not observed in the Newtonian case emerges. The most evident fingerprint of the new dynamics is the slowing down of the annihilation processes which lead to the steady states via weaker kink–antikink interactions. In conclusion, polymers strongly affect the large-scale dynamics. This takes place via a reduction of drag forces we were able to quantify from the asymptotic analysis. This suggests a possible relation of this phenomenon with the dramatic drag-reduction effect taking place in the far turbulent regime.

1. Introduction

A fundamental concept in many fields of science and technology is the coarse-grained description of a system. According to such a concept, a particular system can be described at different levels of detail and the question arising is what is the interrelationship between these levels. Which level is interesting for the description essentially depends on the typical space/time scales on which one wants to focus attention, usually dictated by experimental requirements.

In many cases of interest, ranging from the study of the dynamics of celestial bodies to climatology and biology (see e.g. Khouider, Majda & Katsoulakis 2003; Karrttunen, Vattulainen & Lukkarinen 2004; Vattulainen & Karttunen 2006), the coarse-grained dynamics is ruled by Cahn–Hilliard equations (see Bray 2002). In fluid

mechanics, this class of equations emerges naturally in the study of the nonlinear dynamics of large-scale perturbations. In a variety of situations, it turns out that the evolution of large-scale perturbations is governed by a Cahn–Hilliard equation with a fourth-order potential (see Nepomnyashchyi 1976; Sivashinsky 1985; Pedlosky 1987; Manfroi & Young 1999). The structure of the potential controls the profile and the interactions of the so-called kink–antikink structures observed in snapshots of the flow (She 1987).

In the present paper, we focus our attention on a simple model of viscoelastic flow, the so-called viscoelastic Kolmogorov flow. Its linear stability analysis has been investigated by Boffetta *et al.* (2005*a*). Turbulent regimes and the long-standing problem of drag reduction have been studied by Boffetta *et al.* (2005*b*). Here we perform the intermediate step between the early stage of perturbation evolution and the final turbulent regime. Our main aims are the understanding of the role of polymers on the nonlinear evolution of large-scale perturbations and the possible link between increased stability and drag reduction.

The starting point of our analysis will be results obtained by Boffetta *et al.* (2005*a*) for the linearized stage. The main points are: (i) the most unstable perturbation is of large-scale type and captured by asymptotic methods, at least up to moderate elasticities of the flow; and (ii) the most unstable perturbation is transverse with respect to the basic (Kolmogorov) flow. The same property occurs also in the Newtonian limit.

Here we focus on the weakly nonlinear regime, which amounts to considering values of the Reynolds number close to the marginal stability curve separating stable from unstable regions of the phase-space. Asymptotic methods can be applied as in the Newtonian case with the final result that polymer evolution is found to be ruled by a one-dimensional Cahn–Hilliard equation. The crucial point here is that there exists a critical value of the elasticity at which the order of the Cahn–Hilliard equation passes from cubic to fifth-order. Owing to the one-dimensional character of the nonlinear dynamics (Bray 2002), this transition has important consequences on the dynamics of the large-scale perturbation. In particular, 'hydrodynamic' kink–antikink structures which characterize the dynamics below the transition are replaced above the critical elasticity by generalized kinks and antikinks, whose dynamics turns out to be slower than that of 'standard' kinks and antikinks. Moreover, below the critical value of the elasticity, the mechanism of instability occurs at the level of linear analysis. This amounts to saying that nonlinear terms always tend to stabilize the exponential growth from the linear stage. Above the critical value, we found a purely nonlinear mechanism of instability, which enters into play provided that the initial amplitude of the perturbation is sufficiently large. This instability seems to be akin to other instability mechanisms found in viscoelastic flows in different geometries (Morozov & van Saarloos 2005).

The paper is organized as follows. In §2, we introduce the viscoelastic model considered in the sequel and briefly review the results by Boffetta *et al.* (2005*a*). In §3, we use multiscale methods to derive the coarse-grained equations for the perturbations. In §4, we study the system around the triple critical point and work out the evolution equations in its neighbourhood. In §§5 and 6, we reformulate the asymptotic behaviour of the coarse-grained equations in terms of variational analysis and present the numerical results that corroborate our analytical predictions. Finally, in §7, we address the problem of drag reduction and show that, even for the weakly unstable regime considered here, the injection of polymers induces an enhancement of the mean flow amplitude.

2. Oldroyd-B Kolmogorov flow and linear stability

A popular model for describing the dynamics of polymer solutions is the Oldroyd-B (Oldroyd 1950; Hinch 1977; Bird *et al.* 1987)

$$\partial_t \boldsymbol{v} + (\boldsymbol{v} \cdot \boldsymbol{\partial})\boldsymbol{v} = -\boldsymbol{\partial} p + \nu\beta\partial^2\boldsymbol{v} + \frac{\nu(1-\beta)}{\tau}\boldsymbol{\partial} \cdot (\boldsymbol{\sigma} - 1) + \boldsymbol{f}, \qquad (2.1)$$

$$\partial_t\boldsymbol{\sigma} + (\boldsymbol{v} \cdot \boldsymbol{\partial})\boldsymbol{\sigma} = (\boldsymbol{\partial v})^T \cdot \boldsymbol{\sigma} + \boldsymbol{\sigma} \cdot (\boldsymbol{\partial v}) - \frac{1}{\tau}(\boldsymbol{\sigma} - 1), \qquad (2.2)$$

where $\boldsymbol{v}$ is the incompressible velocity field, $\boldsymbol{\sigma}$ is the symmetric conformation tensor of polymers. The parameter τ is the (slowest) polymer relaxation time. The total kinematic viscosity of the solution is ν, while $\nu\beta$ and $\nu(1-\beta)$ are the separate contributions by the solvent and the polymers, respectively. Their ratio $(1-\beta)/\beta$ is proportional to polymer concentration and will be fixed at the value of 0.3 in the rest of the paper. This corresponds to concentrations commonly used in laboratory experiments.

A substantial simplification comes from the viscoelastic version of Squire's theorem (see Appendix A), stating that, for parallel flows, the most unstable perturbations are two-dimensional. We shall therefore restrict ourselves to a two-dimensional flow (u_x, u_z), without any lack of generality. The constant forcing $\boldsymbol{f} = [F\cos(z/L), 0]$ produces the well-known Kolmogorov flow (Arnold & Meshalkin 1960) $\boldsymbol{v}^{(0)} = (V\cos(z/L), 0)$, where $V = F_0 L^2/\nu$. The corresponding conformation tensor at equilibrium is:

$$\boldsymbol{\sigma}^{(0)} = \begin{pmatrix} 1 + 2\tau^2\dfrac{V^2}{L^2}\sin^2\left(\dfrac{z}{L}\right) & -\tau\dfrac{V}{L}\sin\left(\dfrac{z}{L}\right) \\[12pt] -\tau\dfrac{V}{L}\sin\left(\dfrac{z}{L}\right) & 1 \end{pmatrix}. \qquad (2.3)$$

The two relevant dimensionless numbers in the problem are the Reynolds number $Re = VL/\nu$ and the Deborah number $De = \tau V/L$.

It has long been known that the Newtonian Kolmogorov flow becomes unstable for Reynolds numbers $Re > \sqrt{2}$ (Meshalkin & Sinai 1961); the evolution of large-scale perturbations is formally described by an effective diffusive dynamics, and instabilities are associated to the loss of positive-definiteness of the eddy-viscosity tensor.

In the presence of polymers, performing a multiscale analysis (Bensoussan, Lions & Papanicolau 1978; Bayly, Orszag & Herber 1988) on the linearized Oldroyd-B model, we obtain an explicit expression for the eddy-viscosity tensor, valid for sufficiently low elasticity (Boffetta *et al.* 2005*a*). The resulting stability curve in terms of the Reynolds and the Deborah number is reported in figure 1. The phase-space (Re, De) is divided into a linearly stable region (where the eddy-viscosity tensor is positive-definite) and a region where there exists at least one unstable mode. The complete diagram reveals two kinds of instabilities. When the Deborah number is sufficiently low (as in figure 1), the flow experiences hydrodynamic-like large-scale transverse instabilities. In this region, the critical Reynolds number grows with De, therefore polymers stabilize the flow. This has been interpreted by Boffetta *et al.* (2005*a*), and will be discussed in §7, as a prelude to the drag-reduction effect observed in the turbulent regime.

For high values of the Deborah number (not shown in figure 1), the multiscale analysis predicts the flow to be unstable, even for very low Reynolds numbers. However, numerical simulations show that the assumption of scale separation does not
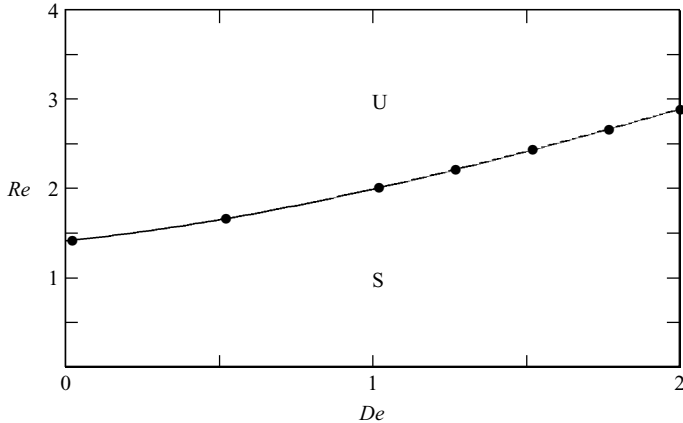
FIGURE 1. The linear stability diagram for $\beta = 0.769$. Stable and unstable regions are denoted by S and U, respectively. The bullets represent the results obtained from a set of direct numerical simulations of the complete Oldroyd-B system of equations, confirming theoretical predictions for this window of parameters.

hold and multiscale techniques are not applicable. This region, possibly characterized by purely elastic instabilities, will not be the concern of the present investigation which focuses on $0 \leqslant De \leqslant 2$.

3. Nonlinear dynamics: the Cahn–Hilliard equation

Linear stability analysis is unable, by definition, to capture the full-time dynamics of unstable perturbations: as the perturbation grows in time, nonlinearities have to be taken into account. We are interested here in studying the nonlinear dynamics of the flow for Reynolds numbers slightly above the linear stability curve.

This problem has been extensively studied in the Newtonian case (Sivashinsky 1985; She 1987; Gama, Vergassola & Frisch 1994). Just above the threshold, large-scale transverse modes become unstable and their dynamics is found to be governed by a one-dimensional Cahn–Hilliard equation (Cahn & Hilliard 1958), a model which emerges in a variety of hydrodynamic situations (see Nepomnyashchyi 1976; Sivashinsky 1985; Pedlosky 1987; Manfroi & Young 1999). In the one-dimensional case, its form reads (see Bray 2002):

$$\frac{\partial w}{\partial t} = \partial_x^2 \frac{\delta F}{\delta w}, \tag{3.1}$$

where $w(\boldsymbol{x}, t)$ is the large-scale field and F a suitable Landau free-energy functional:

$$F[w] = \int \mathrm{d}\boldsymbol{x} \left[\tfrac{1}{2} \lambda |\nabla w|^2 + I(w) \right]. \tag{3.2}$$

The potential $I(w)$ has a double-well structure whose minima correspond to two equilibrium states and λ is some positive constant.

A dynamical description in terms of Cahn–Hilliard equations is expected also in the viscoelastic case, at least for low Deborah numbers (i.e. close to the Newtonian limit).

Our study of the nonlinear dynamics is based on multiscale analysis (Bensoussan *et al.* 1978; Bayly *et al.* 1988). At the basis of the latter approach, it is fundamental to
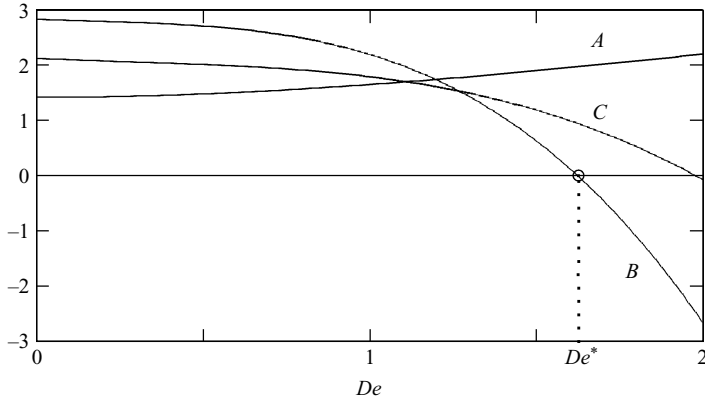
FIGURE 2. The parameters A, B and C appearing in the coarse-grained Cahn–Hilliard equation, (3.4), as a function of the Deborah number (for $\beta = 0.769$).

choose the correct scaling between the slow and fast variables and the scaling of the expansion parameter. Thanks to a global scaling factor, the slow space variable can be defined as $\tilde{x} = \epsilon x$. Space derivatives are then expanded as $\partial_i \to \partial_i + \epsilon \tilde{\partial}_i$. Assuming a Cahn–Hilliard dynamics, in the vicinity of the critical line, i.e. $\nu = \nu_c(1 - \epsilon^2)$, we define a slow time as $\tilde{t} = \epsilon^4 t$ and the dynamical fields are expanded as (Sivashinsky 1985):

$$\boldsymbol{v} = \boldsymbol{v}^{(0)} + \epsilon \boldsymbol{w}^{(1)}(z, \tilde{x}, \tilde{t}) + \epsilon^2 \boldsymbol{w}^{(2)}(z, \tilde{x}, \tilde{t}) + \cdots, \tag{3.3a}$$

$$p = p^{(0)} + \epsilon q^{(1)}(z, \tilde{x}, \tilde{t}) + \epsilon^2 q^{(2)}(z, \tilde{x}, \tilde{t}) + \cdots, \tag{3.3b}$$

$$\boldsymbol{\sigma} = \boldsymbol{\sigma}^{(0)} + \epsilon \boldsymbol{\zeta}^{(1)}(z, \tilde{x}, \tilde{t}) + \epsilon^2 \boldsymbol{\zeta}^{(2)}(z, \tilde{x}, \tilde{t}) + \cdots. \tag{3.3c}$$

The next step for obtaining a coarse-grained equation for the large-scale dynamics is to plug (3.3c) into the Oldroyd-B equations. Exploiting the chain rule, the definitions of $\tilde{x}$ and $\tilde{t}$ and averaging along z, we obtain a set of equations involving solely the large-scale fields. The equation for the large-scale transverse perturbation $\langle w_z^{(1)} \rangle(\tilde{x}, \tilde{t})$ is obtained from the solvability condition at order ϵ^5. The final equation has the form of the 'standard' Cahn–Hilliard equation (for details on the Newtonian case see Gama *et al.* 1994):

$$\tilde{\partial}_t \langle w_z^{(1)} \rangle = \tilde{\partial}_x \left[\left(-A + B \langle w_z^{(1)} \rangle^2 \right) \tilde{\partial}_x \langle w_z^{(1)} \rangle \right] - C \tilde{\partial}_x^4 \langle w_z^{(1)} \rangle. \tag{3.4}$$

The parameters A, B, C are known functions of the parameters De and β, as shown in figure 2. It is worth noting that A is non-negative as the system is supposed to be slightly above the threshold of instability and we have explicitly incorporated a negative sign in (3.4).

The saturation of the instability requires two conditions. First, C must be positive to ensure that the instability be saturated at sufficiently high wavenumbers (still much smaller than those of the basic flow, of order unity). Secondly, B ought to be positive to ensure that, as $\langle w_z^{(1)} \rangle$ becomes $O(\sqrt{A/B})$, the nonlinear eddy-viscosity $-A + B \langle w_z^{(1)} \rangle^2$ changes sign and the growth is again saturated. Both these conditions are satisfied up to a critical value of the Deborah number, De^* (see figure 2).

We conclude this section by stressing that all the fields up to order four are explicitly expressed in terms of the fast variables and of the large-scale field $\langle w_z^{(1)} \rangle$.
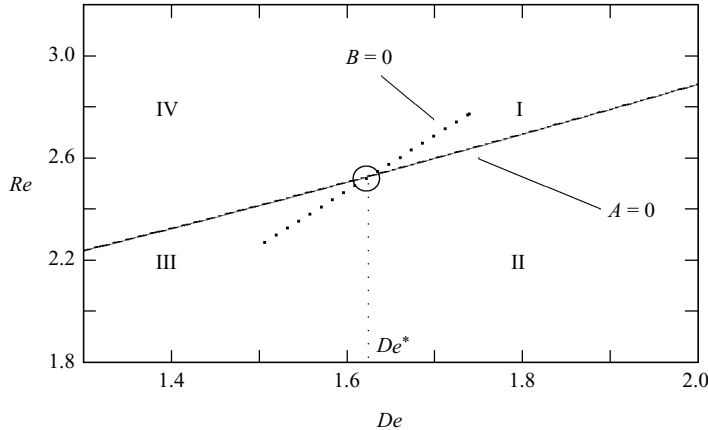
FIGURE 3. The phase-space around the critical point P^* where both the eddy-viscosity and the coefficient of the third-order nonlinearity change sign. The region is divided into four regions schematically sketched here by the two critical curves $A = 0$ and $B = 0$. The former is found from the linear stability analysis in § 3. The latter is found locally, around the $A = 0$ curve, by solving (4.5), and is linearly extrapolated for graphical purposes as a dashed line. For $\beta = 0.769$, the curve $B = 0$ is inclined at approximately $60°$ with respect to the De axis.

4. Generalized Cahn–Hilliard dynamics

Above the critical value of the Deborah number, De^*, the cubic nonlinear term becomes negative. Therefore, the instability keeps growing until the next-order nonlinearity becomes important.

The structure of this next term is dictated by the conservation of momentum and the symmetries of the basic flow (as in Gama *et al.* 1994): $\tilde{\partial}_x(\langle w_z \rangle^4 \tilde{\partial}_x \langle w_z \rangle)$, with a regular coefficient D in the neighbourhood of the critical point P^*, where both the eddy-viscosity and the coefficient of the third-order nonlinearity change sign.

Four regions can be identified around P^* (see figure 3). The eddy-viscosity $A = 0$ curve has been obtained by means of the linear stability analysis (§ 2). The linear approximation of the curve $B = 0$ in the vicinity of P^* is obtained from the analytic expression of B on the marginal curve and the marginal curve itself.

Zone I is linearly unstable ($A > 0$), has a third-order destabilizing term ($B < 0$) and we can guess that a fifth-order term will enter into play to stabilize the growth. Zone II is particularly interesting as it is linearly stable ($A < 0$), but has a third-order destabilizing contribution ($B < 0$). Perturbing with a field of sufficiently strong amplitude, the system jumps to the asymptotic steady state where the two nonlinear terms (third- and fifth-order) balance each other. Zone III is completely stable ($A < 0$, $B > 0$). In the last region, IV, as De approaches the critical value, the coefficient B goes to zero and cannot saturate the exponential growth from the linear instability. The fifth-order nonlinearity, which is negligible far from the critical point, must again enter into play.

4.1. *Zone I*

When both the Reynolds and the Deborah numbers exceed their critical values, previous considerations suggest the following structure for the coarse-grained equation:

$$\tilde{\partial}_t w = -A\tilde{\partial}_x^2 w - |B|\tilde{\partial}_x(w^2\tilde{\partial}_x w) - C\tilde{\partial}_x^4 w + D\tilde{\partial}_x(w^4\tilde{\partial}_x w). \tag{4.1}$$

Confining the analysis to the surroundings of the critical point P^*, we may represent the position in phase space as:

$$\nu = \nu^*\left(1 - K_1\epsilon_\nu - K_2\epsilon_\nu^2\right), \qquad (4.2)$$

$$De = De^*(1 + \epsilon_{De}). \qquad (4.3)$$

Adequately choosing the K_1 and K_2 parameters, any point around P^* can be reached as ϵ varies. The reason why we need to incorporate in (4.2) the additional contribution of order ϵ^2 will be clear shortly.

In the neighbourhood of P^*, the coefficients A and B are expanded as:

$$A = \frac{\partial A}{\partial De}(De - De^*) + \frac{\partial A}{\partial \nu}(\nu - \nu^*), \qquad (4.4)$$

$$B = \frac{\partial B}{\partial De}(De - De^*) + \frac{\partial B}{\partial \nu}(\nu - \nu^*), \qquad (4.5)$$

where all derivatives are computed at P^*.

The scaling in ϵ of the velocity field amplitude, ϵ_w, and the parameters ϵ_ν, ϵ_{De} is found by requiring all terms in (4.1) to be of the same order in the scale-separation small parameter ϵ.

The comparison between the last two terms in (4.1) fixes the relation between ϵ and ϵ_w:

$$D\ \epsilon^2\epsilon_w^5 \sim C\ \epsilon^4\epsilon_w \Rightarrow \epsilon_w = \epsilon^{1/2}. \qquad (4.6)$$

The parameters ϵ_ν and ϵ_{De} are found by comparing the terms associated to A, B and D in (4.1). Using (4.2)–(4.6), we obtain:

$$D\ \epsilon^2\epsilon^{5/2} \sim \left[\frac{\partial A}{\partial De}(\epsilon_{De}De^*) - \frac{\partial A}{\partial \nu}(K_1\epsilon_\nu\nu^*)\right]\epsilon^2\epsilon^{1/2}, \qquad (4.7)$$

$$D\ \epsilon^2\epsilon^{5/2} \sim \left[\frac{\partial B}{\partial De}(\epsilon_{De}De^*) - \frac{\partial B}{\partial \nu}(K_1\epsilon_\nu\nu^*)\right]\epsilon^2\epsilon^{3/2}. \qquad (4.8)$$

Choosing $\epsilon_\nu = \epsilon_{De} = \epsilon$ and setting K_1 to ensure $[(\partial A/\partial De)De^* - (\partial A/\partial \nu)K_1\nu^*] = 0$, both (4.7) and (4.8) are satisfied. Equation (4.7) is balanced by the second-order term of the ν expansion, (4.2), dependent on K_2. The scalings of time, pressure and polymer conformation tensor perturbation, ϵ^4, $\epsilon^{1/2}$ and $\epsilon^{1/2}$, respectively, are derived as discussed in § 3.

Once the scalings have been determined, we can proceed to obtain the large-scale equation for $\langle w_z^{(1/2)}\rangle(\tilde{t}, \tilde{x})$. The evolution equation emerges now from the solvability condition at the order $\epsilon^{9/2}$:

$$\tilde{\partial}_t\langle w_z^{(1/2)}\rangle = \tilde{\partial}_x\left[\left(-A + B\langle w_z^{(1/2)}\rangle^2 + D\langle w_z^{(1/2)}\rangle^4\right)\tilde{\partial}_x\langle w_z^{(1/2)}\rangle\right] - C\tilde{\partial}_x^4\langle w_z^{(1/2)}\rangle, \qquad (4.9)$$

where the coefficients are explicit functions of β. For $\beta = 0.769$, they read:

$$\begin{cases} A = 0.5106 + 1.965K_2, \quad B = -8.979, \\ C = 0.9439, \quad D = 23.11, \quad K_1 = 0.594. \end{cases} \qquad (4.10)$$

Although (4.9) belongs to the class of the Cahn–Hilliard equations (3.1), the emergence of the new sixth-order nonlinearity will be responsible for new dynamical aspects, not present for $De < De^*$, which will be discussed in detail in § 5.

4.2. *Zone II*

For Deborah numbers above the critical value, perturbations are nonlinearly unstable: $B < 0$. This is true regardless of the sign of the linear term and strong enough perturbations may then grow even if the system is linearly stable.

Let us then consider systems with $v > v^*$ and $De > De^*$. No major difference with respect to case I is expected. At zeroth order, the coefficients A and B vanish and equations (4.4)–(4.5) hold. Again, we define the position in phase-space via the two parameters ϵ_v and ϵ_{De}. As the viscosity is now larger than the critical value, a positive sign appears in the expansion of the viscosity:

$$v = v^* \left(1 + K_1 \epsilon_v - K_2 \epsilon_v^2 \right), \tag{4.11}$$

while (4.3) holds. The parameter K_2, as we shall point out later, can take any value compatible with the condition $A > 0$.

The same calculations as discussed in the previous subsection can be carried out to derive the coarse-grained equation for the transverse velocity. As we might expect, its form is exactly the same as (4.9), a generalized Cahn–Hilliard equation. The only difference is in the value of the parameters. For $\beta = 0.769$, they read:

$$\left. \begin{array}{ll} A = -0.2202 + 1.965 K_2, & B = -35.62, \\ C = 0.9439, \quad D = 23.11, & K_1 = 0.5974. \end{array} \right\} \tag{4.12}$$

Only A and B have changed with respect to (4.10), as expected since they are the only parameters which depend on ϵ (and thus on Re and De) in physical coordinates. Notice that there is an upper bound on the values we can choose for K_2, reflecting the linear stability requirement.

4.3. *Zone IV*

What happens when the Deborah number is barely smaller than the critical value De^*? Sufficiently close to it, the third-order instability can be made subdominant with respect to the fifth order and our aim here is to work out the scaling coefficients corresponding to such a situation.

For this purpose, let us assume that the cubic nonlinearity is negligible. At leading order, the terms associated to A, C and D must be of the same order. This means:

$$\epsilon^4 \epsilon_w \sim \epsilon^2 \epsilon_w \left[\frac{\partial A}{\partial De} (De - De^*) + \frac{\partial A}{\partial v} (v - v^*) \right], \tag{4.13}$$

$$\epsilon^2 \epsilon_w^5 \sim \epsilon^2 \epsilon_w \left[\frac{\partial A}{\partial De} (De - De^*) + \frac{\partial A}{\partial v} (v - v^*) \right], \tag{4.14}$$

and implies:

$$v = v^* (1 - K_2 \epsilon^2), \quad De = De^* (1 - \epsilon^2). \tag{4.15}$$

Additionally, the velocity field scales as $\epsilon^{1/2}$, as the pressure and polymer fields do. The time derivative scales as ϵ^4.

To be consistent, we must check that the third-order nonlinearity is negligible. Using the previous scalings and the ensuing fact that $B \sim O(\epsilon^2)$, we have to verify that:

$$O(B \partial^2 w^3) \ll O(D \partial^2 w^5) \Rightarrow O(\epsilon^{11/2}) \ll O(\epsilon^{9/2}), \tag{4.16}$$

which holds true. It is now possible to apply the strategy discussed in §3 to derive the large-scale equation and obtain (at order ϵ^5):

$$\tilde{\partial}_t \langle w_z^{(1/2)} \rangle = \tilde{\partial}_x \left[\left(-A + D \langle w_z^{(1/2)} \rangle^4 \right) \tilde{\partial}_x \langle w_z^{(1/2)} \rangle \right] - C \tilde{\partial}_x^4 \langle w_z^{(1/2)} \rangle, \qquad (4.17)$$

where C and D have the same value as before, and $A = 1.1740 + 1.965 K_2$.

5. Variational formulation

It is well known that the Cahn–Hilliard equation admits a variational formulation in terms of a Ginzburg–Landau potential (Cahn & Hilliard 1958). Equation (3.4), after appropriate rescalings, $w \to (A/B)^{1/2} w$, $t \to A^{-1} t$, $\lambda = C/A$, is recast in the form (3.1) with the Lyapunov functional:

$$F[w] = \int \left[\tfrac{1}{2} \lambda (\partial_x w)^2 + I(w) \right] \mathrm{d}x, \quad I(w) = -\frac{w^2}{2} + \frac{w^4}{12}. \qquad (5.1)$$

Note that mean fields only are considered, that is, w must be read as the rescaled leading contribution $\langle w_z^{(1)} \rangle (\tilde{x}, \tilde{t})$.

The existence of a Lyapunov functional implies the existence of an asymptotic state for w, if boundary conditions are periodic and stationary. Such a state corresponds to a minimum of the Lyapunov functional and it is given by the solution of:

$$I'(w) = \lambda \partial_x^2 w \leftrightarrow \partial_x I = \tfrac{1}{2} \lambda \partial_x (\partial_x w)^2. \qquad (5.2)$$

The boundary conditions for this solution are given by requiring $w = const$ which gives, from $I' = 0$, $w = \pm \sqrt{3}$. With these boundary conditions, the solutions of (5.2) have the well-known kink and anti–kink structures:

$$w = \pm \sqrt{3} \tanh \left[\sqrt{\frac{1}{2\lambda}} x \right]. \qquad (5.3)$$

The issue now is whether or not a Lyapunov extremal formulation exists in the generalized Cahn–Hilliard case, (4.1), as well, and how it relates to the standard one. In particular, a Painlevé test (Ablowitz & Clarkson 1991) can be performed on the equation to check its integrability. The calculation consists in checking that all movable singularities (whose location depends on initial and/or boundary conditions) are poles (see for details Ablowitz & Clarkson 1991). The test is based on a well-known connection between the integrability property of a nonlinear differential equation and its analytic structure for complex values of the independent variable (Kowalevski 1889, 1890; Painlevé 1897). The explicit calculation is performed in Appendix B. The generalized Cahn–Hilliard equation enjoys the Painlevé property and is thus integrable.

Let us then write (4.1) after the rescalings $w \to (A/B)^{1/2} w$, $t \to A^{-1} t$, $\lambda = C/A$, $\gamma = A D/B^2$:

$$\partial_t w = -\partial_x^2 w - \tfrac{1}{3} \partial_x^2 w^3 - \lambda \partial_x^4 w + \tfrac{1}{5} \gamma \, \partial_x^2 w^5. \qquad (5.4)$$

Integrability of this equation is related to the existence of the following Lyapunov functional, similar to that of the standard case, yet with a sixth-order potential:

$$F[w] = \int \left[\tfrac{1}{2} \lambda (\partial_x w)^2 + I(w) \right] \mathrm{d}x, \quad I(w) = -\frac{w^2}{2} - \frac{w^4}{12} + \frac{\gamma}{30} w^6. \qquad (5.5)$$

All solutions tend to final steady states which minimize F. The approach to the solution is, however, non-trivial and the structure is made of plateaux having
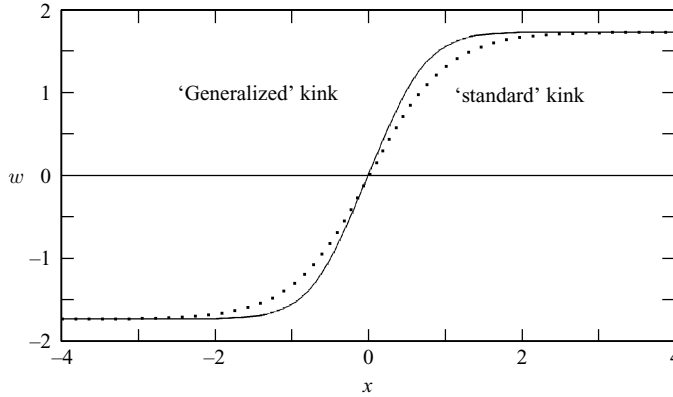
FIGURE 4. The 'generalized' (solid) and 'standard' (dotted) kinks for $\lambda = 1/2$ and $\gamma = 10/9$. The former has a manifestly shorter range. It is shown in the text that this entails longer time scales for their annihilation with the corresponding antikinks.

velocity $\pm W_0$ ($I'(W_0) = 0$), separated by positive and negative kinks (see figure 4). The amplitude of the velocity w in the plateaux is:

$$W_0^2 = \frac{5 + \sqrt{25 + 180\gamma}}{6\gamma}. \tag{5.6}$$

Note that, at small γ, the asymptotic velocity W_0 diverges as $1/\sqrt{\gamma}$. This is intuitive: the field amplitude equilibrating the third- and the fifth-order nonlinearities increases as the coefficient of the fifth-order nonlinearity reduces.

The explicit expression of the profiles for kinks and antikinks is obtained from the integration of (5.2) and (5.5). For example, when $\lambda = 1/2$ and $\gamma = 10/9$, the profiles read:

$$w = \pm\sqrt{15}\frac{\mathrm{e}^{2\sqrt{3}x} - 1}{\sqrt{5\mathrm{e}^{4\sqrt{3}x} + 26\mathrm{e}^{2\sqrt{3}x} + 5}}. \tag{5.7}$$

5.1. Dynamics of generalized kink/antikink annihilation and approach to equilibrium

Detailed calculations are performed following Legras & Villone (2003), who in turn based theirs on Kawasaki & Ohta (1982). They are lengthy, yet simple in their basic idea.

During metastable transitions, the kinks do not satisfy (5.2) exactly, owing to the presence of other kinks and/or antikinks. The deviation of the amplitude in the plateau is proportional to $\mathrm{e}^{-s\Lambda}$, where $\Lambda = 4|x|$ and x denotes the distance to the point where $w = 0$. Here, s is the inverse of the typical length scale of this deviation. The quantity s turns out to be crucial as neighbouring kinks and antikinks attract proportionally to $\mathrm{e}^{-s\Delta x}$, where Δx is the distance between neighbouring kinks and antikinks (for details, see Appendices A and B of Legras & Villone 2003).

The behaviour of the kink size s is understood as follows. Consider a metastable state of the Cahn–Hilliard equation. The potential felt by a kink $w(x)$ close to the plateau $w = W_0$ is estimated by the Taylor expansion:

$$I(w - W_0) \simeq I(W_0) + I'(W_0)(w - W_0) + I''(W_0)\frac{(w - W_0)^2}{2}, \tag{5.8}$$
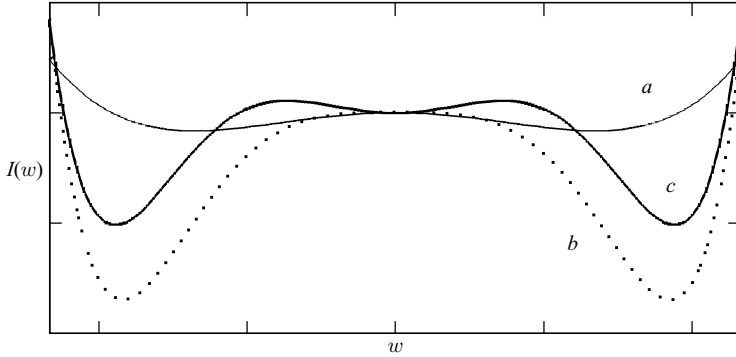
FIGURE 5. The potentials associated to the different evolution equations. Curve *a* is related to the standard Cahn–Hilliard equation (fourth-order potential); curve *b* represents the generalized Cahn–Hilliard equation (sixth-order potential). Curve *c* is the characteristic triple-well potential of the purely nonlinearly unstable case. The plots are in arbitrary units, to ease the comparison between the curves.

where we know that $I'(W_0) = 0$. Note also that the dynamics of w does not change if we add an arbitrary constant to the potential I, so that we can set $I(W_0) \equiv 0$.

Let us now calculate the shape of the profile between w and W_0. For a metastable state, $\partial_t(w - W_0) = 0$, that implies:

$$\frac{\lambda}{2}(\partial_x(w - W_0))^2 + \left[I''(W_0)\frac{(w - W_0)^2}{2}\right] = 0. \tag{5.9}$$

Interpreting ∂_x as the inverse of the typical length scale s for $(w - W_0)$, we easily obtain $s = \sqrt{\lambda/I''(W_0)}$. The second-order derivative can be explicitly calculated using (5.6):

$$I''(W_0) = 4 + \tfrac{2}{3}W_0^2. \tag{5.10}$$

Qualitative properties of s are easy to grasp. At large γ, the size of the kinks tends to a constant, independent of γ. At small γ, the kinks become steeper and steeper, their size scaling as $\gamma^{1/2}$. This implies that the convergence to equilibrium will be slower and slower as γ is reduced (recall that the kinks attract proportionally to $e^{-s\Delta x}$).

For the same band of unstable modes, i.e. keeping λ fixed, it holds that the convergence to equilibrium is slower for the generalized than for the standard Cahn–Hilliard equation. Indeed, for the Cahn–Hilliard potential $I_{CH} = -w^2/2 + w^4/12$, the second-order derivative $I''_{CH}(W_0) = 2$. As for (5.10), we can use the identity $1 + W_0^2/3 = \gamma W_0^4/5$, following from the definition $I'(W_0) = 0$, to obtain $I''(W_0) > 2$. This implies that the interactions for the generalized kink–antikink structures have a shorter range and their dynamics of annihilation is thus slower.

A special remark applies to the linearly stable case (zone II). In this case, the equation is associated to an uncommon triple-well potential (figure 5). The typical nonlinear kink–antikink dynamics appears only if the initial perturbation is energetic enough to let the system 'jump' out of the central well and fall into one of the side wells.
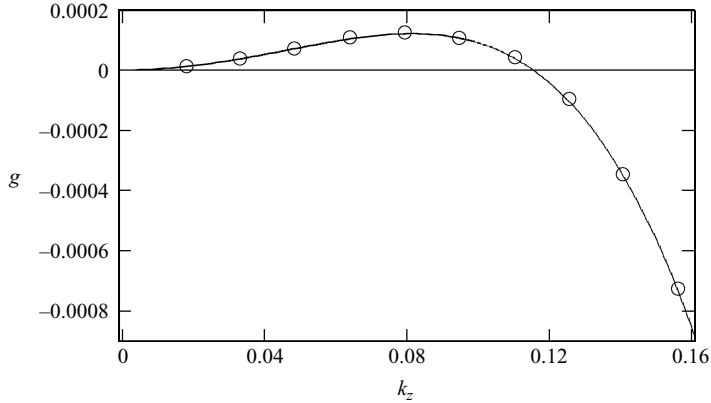
FIGURE 6. Growth rates g of the transverse Fourier modes k for a simulation with $De = 1.4$ and $\beta = 0.769$. The simulations are performed in a rectangular domain with aspect ratio $1/64$. The distance from the critical line is $Re = 1.28 Re_c$. The solid line represents the linear prediction (6.1). The circles representing the numerically computed growth rates have been obtained with a DNS simulation by a linear fit of the logarithm of the energy for each mode versus time, in the early stages of their exponential growth.

6. Numerical results

The analytical results presented in this work have been obtained by multiscale techniques. Their basic assumption is the strong scale separation between the basic flow and the most unstable perturbations. In this section, we shall present numerical simulations performed to check the validity of this assumption. To this aim, we have numerically integrated the complete Oldroyd-B model equations (2.1)–(2.2) on a doubly periodic box of size $L_x = 128\pi$, $L_z = 2\pi$ at resolution 256×32. The high aspect ratio is fundamental as we have a small-scale primary flow along z and a large-scale secondary flow along x. The integration was carried on by a standard pseudo-spectral code and will be referred to as direct numerical simulations (DNS). We have also integrated the one-dimensional Cahn–Hilliard (CH) equation, again with a pseudo-spectral code at resolution 256 (CH simulations).

The first check of our results concerns the growth rates of the instability which, in the linear regime, can be obtained by the Cahn–Hilliard equation. Neglecting the nonlinear term, the dispersion relation for the transverse Fourier modes k is:

$$g = A\left(\frac{Re}{Re_c} - 1\right)k^2 - Ck^4. \tag{6.1}$$

In figure 6, we report the growth rates of the first modes for a (white-noise in space) small initial perturbation. We are then able to observe also negative g (stable modes). The comparison with the linear prediction is excellent, even for modes whose scale separation is not very small.

Let us now consider the nonlinear stage of the perturbation growth. It is well known that the time evolution of the Cahn–Hilliard equation shows a succession of long-lasting metastable states characterized by a well-defined periodicity. For sufficiently small initial perturbations, the wavenumber k associated to the maximum growth-rate g will be the first to reach the balance between the destabilizing linear term $A\tilde{\partial}^2\langle w_z\rangle$ and the stabilizing nonlinear one $B\tilde{\partial}^2\langle w_z\rangle^3$. When such equilibrium is reached, the
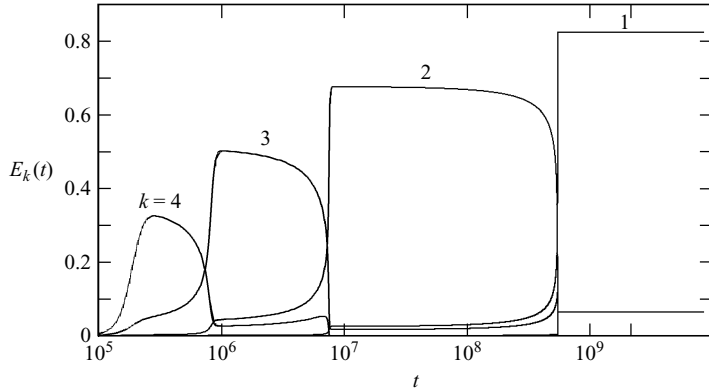
FIGURE 7. The energy associated to the lowest wavenumber modes as a function of time, resulting from a CH simulation. The quasi-stationary states can be clearly seen up to the asymptotic one corresponding to the largest periodicity. In this simulation, $De = 1.4$ and $Re/Re_c - 1 = 0.28$.
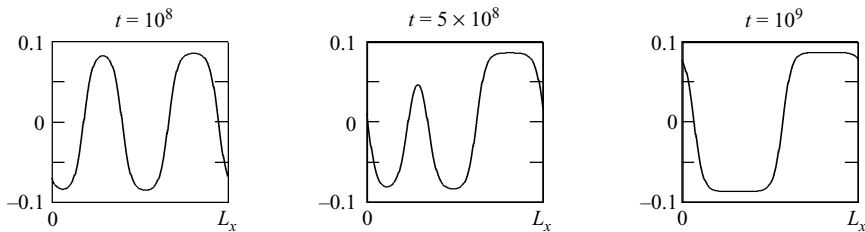
FIGURE 8. Instantaneous transverse velocity field at different times. Parameters are the same as figure 7. Transitions between two metastable states can be regarded as kink–antikink annihilation. In this figure, a transition from a $k = 2$ to a $k = 1$ state is represented. Times correspond to the evolution shown in figure 7.

energy associated to that mode is constant and the system is quasi-stable. In the meanwhile, the other modes $k_{max} - 1, k_{max} - 2, \dots$ keep growing. When the mode $k_{max} - 1$ balances the two terms, the energy associated to the mode k_{max} drops. This new state is again quasi-stationary and has a well-defined periodicity $k_{max} - 1$. The process continues until a state with the box periodicity is reached (see figure 7); such a state is stationary and corresponds to the asymptotic behaviour in §5. Transition between quasi-stationary states can be seen as a kink–antikink annihilation, yielding a decrease in periodicity, as shown in figure 8.

In order to check the results obtained in §3, we have performed a DNS simulation for a particularly long lapse of time. The excellent agreement between the DNS and the prediction of the Cahn–Hilliard equation is shown in figure 9.

The same comparison can be realized in the neighbourhood of the critical point P^*. This kind of simulation is more difficult than for the standard Cahn–Hilliard, because it involves a precise knowledge of the position of the critical point, and there is no easy way to obtain this from the simulations. Moreover, any system we simulate will be at a finite distance from the critical point. The parameter that will mostly feel this difference will be D, as we have chosen it to be approximately constant around
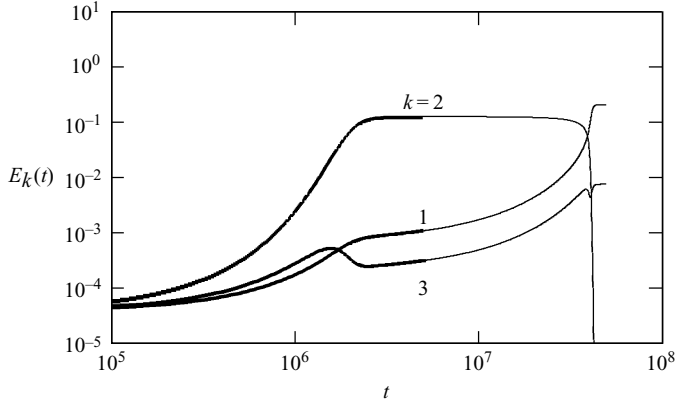
FIGURE 9. The comparison between DNS simulations of the Oldroyd-B model and the coarse-grained Cahn–Hilliard equation derived in the text. Thicker lines represent the evolution of the lowest-energy modes in a DNS simulation, while the thinner lines are the result of a CH simulation. Parameters have been set in the Cahn–Hillard regime, $De = 1.4 < De^*$, $\beta = 0.769$ and $Re = 1.14 Re_c$.
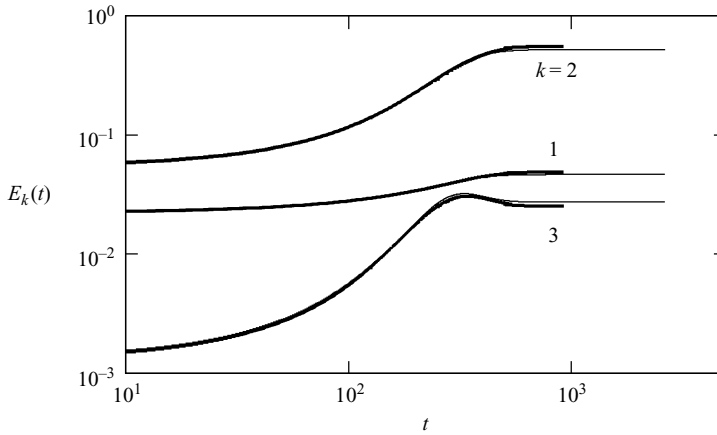
FIGURE 10. The generalized Cahn–Hilliard equation reproduces the dynamics of the Oldroyd-B model around the critical point P^*. Thicker lines represent DNS simulations while the thinner ones are CH simulations. Parameters correspond to the generalized Cahn–Hillard regime, $De = 1.62 > De^*$, $Re = 2.516$.

P^*. We have been able to overcome this weakness via a limited tweaking of the D parameter in the CH simulation. As shown in figure 10, excellent agreement between the curves is again achieved.

7. Clues on drag reduction

One of the most striking properties of viscoelastic fluids is the drag-reduction effect. In 1949, Toms found that the injection of minute amounts of polymers in turbulent fluids flowing in a channel could reduce the turbulent drag up to 80%. Even through this phenomenon has been known for over fifty years (Toms 1949; Lumley 1969; Virk 1975), a satisfactory understanding of its fundamental mechanisms is still lacking.

A large number of experiments have been performed to study this effect (see, e.g. Virk 1975; Nadolink & Haigh 1995; Sreenivasan & White 2000), but a burst in its theoretical analysis occurred after drag reduction was found in numerical simulations of viscoelastic fluids (Sureshkumar, Beris & Handler 1997). The activity is being spurred on both by fundamental interest and industrial applications (Larson 1992).

Drag reduction is commonly associated to channel flows and boundary effects. Still, it is now clear that the phenomenon is present even in the absence of boundaries (Boffetta *et al.* 2005*b*). What we show here is that, even at relatively small Reynolds numbers, where the flow is non-turbulent, an increase in the Deborah number produces an enhancement in the mean flow amplitude. Simply by looking at the linear stability diagram (figure 1), we may already conclude that, as the polymer elasticity grows, so does the critical Reynolds number and therefore the flow is stabilized. Let us further investigate this effect analytically using the results of §3.

The drag coefficient f can be defined in terms of the mean flow properties as (Boffetta *et al.* 2005*b*):

$$f = \frac{F_0 L}{U^2}, \tag{7.1}$$

and can be seen as the ratio between the energy input (through the forcing F_0) and the mean energy of the flow. As we are interested in mean effects only, we will average U^2 over the basic flow periodicity. This will ensure that only mean effects will be taken into account.

When the state is linearly stable (low Reynolds numbers) we have $V = F_0 L^2/\nu$ and therefore $f = Re^{-1}$.

In §3, we have solved all the equations of motion up to the fourth order. We can then write the primary flow as a sum of terms, the first of which is the basic Kolmogorov flow, and the others are functions of the transverse perturbation field. Upon averaging over all possible initial conditions, an equation for the primary flow can be easily obtained:

$$\overline{U_x(z)} = \left(V + h(De, \beta) \frac{\overline{\langle w_z^{(1)} \rangle^2}}{V} \right) \cos\left(\frac{z}{L}\right) = V_{\text{eff}} \cos\left(\frac{z}{L}\right), \tag{7.2}$$

where h is an explicit function of the Deborah number and the quantity $\overline{\langle w_z^{(1)} \rangle^2}$ follows from the Cahn–Hilliard equation in the stationary state and is equal to $\sqrt{3\epsilon^2 A/B}$.

Since the analytical expression of A and B is known, as well as how ϵ changes with De for a fixed Reynolds number, the analytical expression for f is obtained:

$$f = \frac{\nu F L}{V_{\text{eff}}^2} = \frac{V^2}{Re V_{\text{eff}}^2} = \frac{1}{Re\left(1 + h \dfrac{3A}{BV^2} \dfrac{Re - Re_c}{Re_c}\right)^2}, \tag{7.3}$$

where h, A, B and Re_c are explicit functions of the Deborah number.

As we want to investigate how the polymer elasticity affects the flow, a meaningful approach is to keep the Reynolds number fixed, while varying the Deborah number. This allows us to study how the same flow reacts when different kinds of polymers are injected. Once β and Re are chosen, it is possible to plot f versus De on the basis of analytical results (figure 11). The drag coefficient is clearly decreasing with the Deborah number. This permits us to conclude that, although the flow is barely in
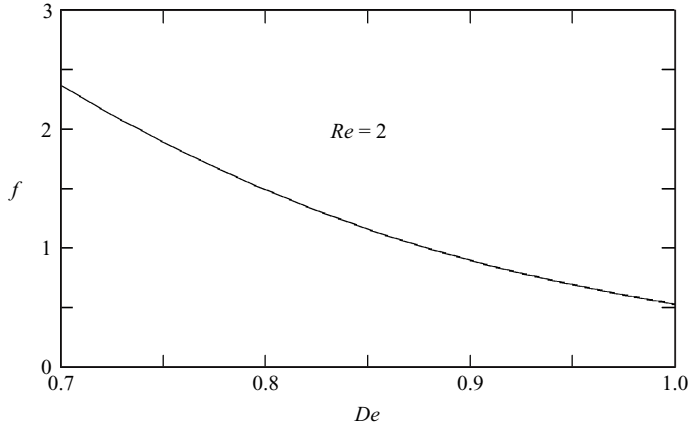
FIGURE 11. The drag coefficient f versus the Deborah number De at constant Re. As the polymer elasticity grows, the drag coefficient diminishes. This implies that the mean flow grows with De.

its nonlinear regime, and thus far from a turbulent regime, a seed of drag reduction induced by polymer is already evident in the present stage.

8. Conclusions

The weakly nonlinear dynamics of a viscoelastic Kolmogorov flow has been studied both analytically and numerically. The physical reason for considering this flow is that it has several analogies with channel flows, despite the absence of material boundaries, and it is one of the few known exact solutions of the Oldroyd-B model.

The weakly nonlinear regime amounts to considering values of the Reynolds number close to the marginal stability curve separating stable from unstable regions of the phase-space. In the general nonlinear case (i.e. for arbitrarily large distances from the marginal curve), there is no way to solve the fully nonlinear equations. Conversely, close to the marginal line, asymptotic perturbation techniques can be employed to capture the weakly nonlinear dynamics.

We found that the weakly nonlinear dynamics is described by Cahn–Hilliard-like equations, with coefficients dependent on the Deborah number. The behaviour of these coefficients with respect to De reveals that there exists a critical value of the Deborah number, where the system bifurcates to another regime. The resulting nonlinear equation still has a Cahn–Hilliard form, but contains a novel fifth-order nonlinearity. A system with a similar phenomenology is the stratified Kolmogorov flow investigated by Balmforth & Young (2005), with the role of elasticity played by stratification.

Above the critical De, the 'hydrodynamic' kink–antikink structures are replaced by generalized structures. We have shown that their processes of annihilation are slowed down with respect to the standard Cahn–Hilliard equation. We also found a purely nonlinear, subcritical mechanism of instability, which occurs for sufficiently large amplitudes of the initial perturbation.

Our results have been obtained both by exploiting the multiscale expansion and via direct numerical simulations of the original equations and their coarse-grained version. The agreement between the Cahn–Hilliard dynamics and the fully resolved

simulations is excellent even at large times. Therefore the asymptotic analysis is able to capture all the relevant features of the flow.

In the last part of the work, we have presented some conjectures on the relevance of this problem for drag reduction. Although it is not common to consider this effect in non-turbulent flows, we have shown that, even in the weakly nonlinear case, the injection of polymers induces an increase of the mean flow and thus a reduction in the drag coefficient. Using the results of the nonlinear analysis, we have been able to give an analytical expression for the flow enhancement due to the polymers. The main qualitative conclusion, which could be relevant also for the turbulent regime, is that drag reduction appears to be a phenomenon coupling large and small scales.

Appendix A. Squire's theorem for Oldroyd-B

Consider a parallel flow $U = (U(z), 0)$. To investigate its stability properties, we write the linearized non-dimensional equations

$$\partial_t \boldsymbol{w} + (\boldsymbol{u} \cdot \nabla)\boldsymbol{w} + (\boldsymbol{w} \cdot \nabla)\boldsymbol{u} = -\nabla q + \beta Re^{-1} \Delta \boldsymbol{w}$$
$$+ (1 - \beta) Re^{-1} De^{-1} \nabla \cdot \boldsymbol{\zeta}, \qquad (A\,1)$$

$$\partial_t \boldsymbol{\zeta} + (\boldsymbol{u} \cdot \nabla)\boldsymbol{\zeta} + (\boldsymbol{w} \cdot \nabla)\boldsymbol{\sigma} = (\nabla \boldsymbol{u})^T \cdot \boldsymbol{\zeta} + (\nabla \boldsymbol{w})^T \cdot \boldsymbol{\sigma}$$
$$+ \boldsymbol{\zeta} \cdot (\nabla \boldsymbol{u}) + \boldsymbol{\sigma} \cdot (\nabla \boldsymbol{w}) - De^{-1} \boldsymbol{\zeta}, \qquad (A\,2)$$

where $\boldsymbol{w}$ is the perturbation of the basic profile $\boldsymbol{u}$, and $\boldsymbol{\zeta}$ is the perturbation of the basic stress tensor $\boldsymbol{\sigma}$.

We now perform a Fourier transform in the directions x and y, and in time,

$$w_i(x, y, z, t) = \int d\omega \, dk_x \, dk_y \, \exp\left(-i\omega t + k_x x + k_y y\right) \hat{w}_i(k_x, k_y, \omega, z), \qquad (A\,3)$$

$$\zeta_{ij}(x, y, z, t) = \int d\omega \, dk_x \, dk_y \, \exp\left(-i\omega t + k_x x + k_y y\right) \hat{\zeta}_{ij}(k_x, k_y, \omega, z). \qquad (A\,4)$$

Introducing the notation

$$\left.\begin{array}{l}
\boldsymbol{k} = \begin{pmatrix} k_x \\ k_y \end{pmatrix}, \quad \boldsymbol{u} = \begin{pmatrix} U(z) \\ 0 \end{pmatrix}, \quad \hat{\boldsymbol{w}} = \begin{pmatrix} \hat{w}_x \\ \hat{w}_y \end{pmatrix}, \\[12pt]
\hat{\boldsymbol{t}} = \begin{pmatrix} \hat{\zeta}_{xz} \\ \hat{\zeta}_{yz} \end{pmatrix}, \quad \hat{\boldsymbol{z}} = \begin{pmatrix} \hat{\zeta}_{xx} & \hat{\zeta}_{xy} \\ \hat{\zeta}_{yx} & \hat{\zeta}_{yy} \end{pmatrix}, \quad \boldsymbol{r} = \begin{pmatrix} \sigma_{xz} \\ \sigma_{yz} \end{pmatrix}, \quad \boldsymbol{s} = \begin{pmatrix} \sigma_{xx} & \sigma_{xy} \\ \sigma_{yx} & \sigma_{yy} \end{pmatrix},
\end{array}\right\} \quad (A\,5)$$

the linearized equations in normal modes take the form

$$(-i\omega + i\boldsymbol{k}^T \cdot \boldsymbol{u})\hat{\boldsymbol{w}} + \hat{w}_z \frac{d\boldsymbol{u}}{dz} = -i\boldsymbol{k}\hat{q} + \beta Re^{-1}\left(-\boldsymbol{k}^2 + \frac{d^2}{dz^2}\right)\hat{\boldsymbol{w}}$$
$$+ (1 - \beta) Re^{-1} De^{-1}\left(i\hat{\boldsymbol{z}}^T \cdot \boldsymbol{k} + \frac{d}{dz}\hat{\boldsymbol{t}}\right), \qquad (A\,6)$$

$$(-i\omega + i\mathbf{k}^T \cdot \mathbf{u})\hat{w}_z = -\frac{d\hat{q}}{dz} + \beta Re^{-1}(-\mathbf{k}^2 + \frac{d^2}{dz^2})\hat{w}_z$$
$$+ (1 - \beta)\, Re^{-1}\, De^{-1}\left(i\mathbf{k}^T \cdot \hat{\mathbf{t}} + \frac{d}{dz}\hat{\zeta}_{zz}\right), \quad (A\,7)$$

$$(-i\omega + i\mathbf{k}^T \cdot \mathbf{u} + De^{-1})\hat{\mathbf{z}} + \hat{w}_z\frac{d}{dz}\mathbf{s} = \hat{\mathbf{t}} \cdot \frac{d\mathbf{u}^T}{dz} + \frac{d\mathbf{u}}{dz} \cdot \hat{\mathbf{t}}^T$$
$$+ i(\mathbf{s} \cdot \mathbf{k})\hat{\mathbf{w}}^T + i\hat{\mathbf{w}}(\mathbf{k}^T \cdot \mathbf{s}) + r\frac{d}{dz}\hat{\mathbf{w}}^T + \frac{d\hat{\mathbf{w}}}{dz}\mathbf{r}^T, \quad (A\,8)$$

$$(-i\omega + i\mathbf{k}^T \cdot \mathbf{u} + De^{-1})\hat{\mathbf{t}} + \hat{w}_z\frac{d}{dz}\mathbf{r} = \hat{\zeta}_{zz}\frac{d\mathbf{u}}{dz}$$
$$+ i(\mathbf{s} \cdot \mathbf{k})\hat{w}_z + i\hat{\mathbf{w}}(\mathbf{r}^T \cdot \mathbf{k}) + r\frac{d}{dz}\hat{w}_z + \frac{d}{dz}\hat{\mathbf{w}}, \quad (A\,9)$$

$$(-i\omega + i\mathbf{k}^T \cdot \mathbf{u} + De^{-1})\hat{\zeta}_{zz} = 2i(\mathbf{r}^T \cdot \mathbf{k})\hat{w}_z + 2\frac{d}{dz}\hat{w}_z. \quad (A\,10)$$

Consider the following transformation

$$\begin{aligned}
\bar{k}_x &= |\mathbf{k}|, & \overline{w}_x &= \frac{\mathbf{k}^T \cdot \hat{\mathbf{w}}}{|\mathbf{k}|}, & \overline{w}_z &= \hat{w}_z, & \bar{q} &= \frac{|\mathbf{k}|}{k_x}\hat{q}, \\
\overline{Re} &= \frac{k_x}{|\mathbf{k}|}Re, & \overline{De} &= \frac{k_x}{|\mathbf{k}|}De, & \bar{\omega} &= \frac{|\mathbf{k}|}{k_x}\omega, \\
\bar{t}_x &= \frac{k_x}{|\mathbf{k}|}\frac{\mathbf{k}^T \cdot \hat{\mathbf{t}}}{|\mathbf{k}|}, & \bar{\zeta}_{xx} &= \frac{k_x}{|\mathbf{k}|}\frac{\mathbf{k}^T \cdot \hat{\mathbf{z}} \cdot \mathbf{k}}{|\mathbf{k}|^2}, & \bar{\zeta}_{zz} &= \frac{k_x}{|\mathbf{k}|}\hat{\zeta}_{zz}.
\end{aligned} \right\} \quad (A\,11)$$

From (A 6)–(A 10), we can derive the equations for the variables withoverbars

$$[-i\bar{\omega} + i\bar{k}_x U(z)]\overline{w}_x + \overline{w}_z\frac{dU}{dz} = -i\bar{k}_x\bar{q} + \beta\overline{Re}^{-1}\left(-\bar{k}_x^2 + \frac{d^2}{dz^2}\right)\overline{w}_x$$
$$+ (1-\beta)\overline{Re}^{-1}\overline{De}^{-1}\left(i\bar{k}_x\bar{\zeta}_{xx} + \frac{d}{dz}\bar{t}_x\right), \quad (A\,12)$$

$$[-i\bar{\omega} + i\bar{k}_x U(z)]\overline{w}_z = -\frac{d\bar{q}}{dz} + \beta\overline{Re}^{-1}\left(-\bar{k}_x^2 + \frac{d^2}{dz^2}\right)\overline{w}_z$$
$$+ (1-\beta)\overline{Re}^{-1}\overline{De}^{-1}\left(i\bar{k}_x\bar{t}_x + \frac{d}{dz}\bar{\zeta}_{zz}\right), \quad (A\,13)$$

$$[-i\bar{\omega} + i\bar{k}_x U(z) + \overline{De}^{-1}]\bar{\zeta}_{xx} + \overline{w}_z\frac{d\bar{s}_{xx}}{dz} = 2\bar{t}_x\frac{dU}{dz} + 2i\bar{k}_x\bar{s}_{xx}\overline{w}_x + 2\bar{r}_x\frac{d\overline{w}_x}{dz}, \quad (A\,14)$$

$$[-i\bar{\omega} + i\bar{k}_x U(z) + \overline{De}^{-1}]\bar{t}_x + \overline{w}_z\frac{d}{dz}\bar{r}_x = \bar{\zeta}_{zz}\frac{dU}{dz} + i\bar{s}_{xx}\bar{k}_x\overline{w}_z + i\bar{k}_x\overline{w}_x\bar{r}_x$$
$$+ \bar{r}_x\frac{d\overline{w}_z}{dz} + \frac{d\overline{w}_x}{dz}, \quad (A\,15)$$

$$[-i\bar{\omega} + i\bar{k}_x U(z) + \overline{De}^{-1}]\bar{\zeta}_{zz} = 2i\bar{k}_x\bar{r}_x\overline{w}_z + 2\frac{d\overline{w}_z}{dz}, \quad (A\,16)$$

where we introduced the quantities

$$\bar{s}_{xx} = \frac{\mathbf{k}^T \cdot \mathbf{s} \cdot \mathbf{k}}{|\mathbf{k}|^2} = 1 + \overline{De}^2[U'(z)]^2, \quad \bar{r}_x = \frac{\mathbf{k}^T \cdot \mathbf{r}}{|\mathbf{k}|} = \overline{De}^2 U'(z). \quad (A\,17)$$

Equations (A 12)–(A 16) are exactly the same as (A 6)–(A 10) but with $k_y = 0$, $\hat{w}_y = 0$, $\zeta_{xy} = \zeta_{yy} = \zeta_{yz} = 0$. Therefore they describe a two-dimensional linear disturbance of the basic flow at smaller Reynolds and Deborah numbers. If the three-dimensional perturbation $\boldsymbol{w}, \boldsymbol{\zeta}$ is unstable at (Re, De), then the two-dimensional disturbance $\overline{\boldsymbol{w}}, \overline{\boldsymbol{\zeta}}$ is unstable at $(\overline{Re}, \overline{De})$ and its rate of growth is larger ($\mathrm{Im}(\overline{\omega}) \geqslant \mathrm{Im}(\omega) > 0$).

Appendix B. Painlevé analysis

We perform a Painlevé analysis to ascertain whether the fifth-order equation (4.1) is integrable as the usual cubic Cahn–Hilliard equation (3.4).

After rescaling dependent and independent variables, the stationary equation takes the form:

$$-u - \frac{u^3}{3} - \lambda \partial_x^2 u + \frac{\gamma}{5} u^5 = 0. \tag{B 1}$$

The Painlevé test consists in checking whether the structure of the solution around singularities in the complex plane has the form of a Laurent series. A simple balance of the last two terms in the equation indicates that the singularity has order $-1/2$. The putative Laurent series should then be sought as:

$$u(z) = z^{-1/2}[u_0 + u_1 z + u_2 z^2 + u_3 z^3 + \cdots], \tag{B 2}$$

where z is the complex variable denoting the separation from the singularity z_*. When the series (B 2) is inserted into equation (B 1), a hierarchy of equations of the form $a_k u_k = b_k$ is obtained. a_k and b_k can be calculated in terms of $u_{k-1}, \ldots, u_0$. The impossibility of an arbitrary equation having a Laurent series expansion is due to resonances, i.e. values of k such that $a_k = 0$. Integrability is equivalent to checking that $b_k = 0$ for the orders corresponding to resonances. In our case, it is easy to check that

$$a_k = -\lambda\left(k - \tfrac{1}{2}\right)\left(k - \tfrac{3}{2}\right) + \gamma u_0^4, \quad u_0 = \left(\frac{15\lambda}{4\gamma}\right)^{1/4} \mapsto a_k = -\lambda(k+1)(k-3). \tag{B 3}$$

The resonance is therefore at the third order and we must perform the explicit calculation up to that order to check whether or not $b_3 = 0$. The algebra is elementary and the coefficients are:

$$u_1 = \frac{u_0^3}{12\lambda}, \quad u_2 = \frac{u_0}{\lambda}\left[\frac{1}{3} + \frac{5}{128\gamma}\right]. \tag{B 4}$$

Using these values, we can verify that

$$b_3 = 2\gamma u_0^2 u_1^3 + 4\gamma u_0^3 u_1 u_2 - u_1 - u_0^2 u_2 - u_0 u_1^2 \tag{B 5}$$

vanishes and the Painlevé test is satisfied.

REFERENCES

ABLOWITZ, M. J. & CLARKSON, P. A. 1991 *Solitons, Nonlinear Evolution Equations and Inverse Scattering.* Cambridge University Press.

ARNOLD, V. I. & MESHALKIN, L. 1960 A. N. Kolmogorov's seminar on selected problems of analysis (1958–1959). *Uspekhi Mat. Nauk.* **15**, 247–250.

BALMFORTH, N. J., YOUNG, Y.-N. 2005 Stratified Kolmogorov flow. Part 2. *J. Fluid Mech.* **528**, 23–42.

BAYLY, B. J., ORSZAG, S. A. & HERBER, T. 1988 Instability mechanisms in shear-flow transition. *Annu. Rev. Fluid Mech.* **20**, 359–391.

BENSOUSSAN, A., LIONS, J.–L. & PAPANICOLAU, G. 1978 *Asymptotic Analysis for Periodic Structures.* North–Holland.

Bird, R. B., Hassager, O., Armstrong, R. C. & Curtiss, C. F. 1987 *Dynamics of Polymeric Liquids*. Wiley.

Boffetta, G., Celani, A., Mazzino, A., Puliafito, A. & Vergassola, M. 2005a The viscoelastic Kolmogorov flow: eddy viscosity and linear stability. *J. Fluid Mech.* **523**, 161–170.

Boffetta, G., Celani, A. & Mazzino, A. 2005b Drag reduction in the turbulent Kolmogorov flow. *Phys. Rev.* E **71**, 036307.

Bray, A. J. 2002 Theory of phase-ordering kinetics. *Adv. Phys.* **51**, 481587.

Cahn, J. W. & Hilliard, J. E. 1958 Free energy of a non uniform system. *J. Chem. Phys.* **28**, 258.

Gama, S., Vergassola, M. & Frisch, U. 1994 Negative eddy-viscosity in isotropically forced two-dimensional flow: linear and nonlinear dynamics. *J. Fluid Mech.* **260**, 95–126.

Hinch, E. J. 1977 Mechanical models of dilute polymer solutions in strong flows. *Phys. Fluids* **20**, S22–S30.

Karttunen, M., Vattulainen, I. & Lukkarinen, A. 2004 *Novel Methods in Soft Matter Simulations*. Springer.

Kawasaki, K. & Ohta, T. 1982 Kink dynamics in one-dimensional nonlinear systems. *Physica* A **116**, 573.

Khouider, B., Majda, A. J. & Katsoulakis, M. A. 2003 Coarse-grained stochastic models for tropical convection and climate. *Proc. Natl Acad. Sci.* **100**, 1194111946.

Kowalesvki, S. 1889 Sur le problème de la rotation d'un corps solide autour d'un point fixe. *Acta Math.* **12**, 177–232.

Kowalesvki, S. 1890 Sur une propriété du système d'équations différentielles qui définit la rotation d'un corps solide autour d'un point fixe. *Acta Math.* **14**, 81–93.

Larson, R. G. 1992 Instabilities in viscoelastic flows. *Rheol. Acta* **31**, 213–263.

Legras, B. & Villone, B. 2003 Dispersive and friction-induced stabilization of the Cahn–Hilliard inverse cascade. *Physica* D **175**, 139–166.

Lumley, J. 1969 Drag reduction by additives. *Annu. Rev. Fluid Mech.* **1**, 367–384.

Manfroi, A. & Young, W. 1999 Slow evolution of zonal jets on the beta-plane. *J. Atmos. Sci.* **56**, 784–800.

Meshalkin, L. & Sinai, Ya. G. 1961 Investigation of the stability of a stationary solution of a system of equations for the plane movement of an incompressible viscous fluid. *Z. Angew. Math. Mech.* **25**, 1700–1705.

Morozov, A. N. & van Saarloos, W. 2005 Subcritical finite-amplitude solutions in plane Couette flow of visco-elastic fluids. *Phys. Rev. Lett.* **95**, 024501.

Nadolink, R. H. & Haigh, W. W. 1995 Bibliography on skin friction reduction with polymers and other boundary-layer additives. *Appl. Mech. Rev.* **48**, 351–460.

Nepomnyashchyi, A. A. 1976 On the stability of the secondary flow of a viscous fluid in an infinite domain. *Appl. Math. Mech.* **40**, 886–891.

Oldroyd, J. G. 1950 On the formulation of rheological equations of state. *Proc. R. Soc. Lond.* A **200**, 523–541.

Painlevé, P. 1897 *Leçons sur la Théorie Analytique des Équations Differentielles*. Hermann, Paris.

Pedlosky, J. 1987 *Geophysical Fluid Dynamics* 2nd edn. Springer.

She, Z. S. 1987 Metastability and vortex pairing in the Kolmogorov flow. *Phys. Lett.* A **124**, 161–164.

Sivashinsky, G. I. 1985 Weak turbulence in periodic flows. *Physica* D **17**, 243–255.

Sreenivasan, K. R. & White, C. M. 2000 The onset of drag reduction by dilute polymer additives, and the maximum drag reduction asymptote. *J. Fluid Mech.* **409**, 149–164.

Sureshkumar, R., Beris, A. N. & Handler, R. A. 1997 Direct numerical simulation of polymer-induced drag reduction in turbulent channel flow. *Phys. Fluids* **9**, 743–755.

Toms, B. A. 1949 Observation on the flow of linear polymer solutions through straight tubes at large Reynolds numbers. *Proc. 1st International Congress on Rheology* **2**, 135–141.

Vattulainen, I. & Karttunen, M. 2006 *Handbook of Theoretical and Computational Nanotechnology* (ed. M. Rieth & W. Schommers). American Scientific Press.

Virk, P. S. 1975 Drag reduction fundamentals. *AIChE J.* **21**, 625–656.